J Appl Electrochem (2009) 39:2489–2496
DOI 10.1007/s10800-009-9940-0

ORIGINAL PAPER

Comparison of anodic dissolution, surface brightness and surface roughness of nanocrystalline nickel coatings with conventional decorative chromium coatings

P. Najafi Sayar · M. E. Bahrololoom

Received: 8 December 2008 / Accepted: 7 June 2009 / Published online: 19 June 2009

Abstract The effects of saccharin concentration and pulsating peak current density on corrosion behaviour, surface brightness and surface roughness of nanocrystalline nickel coatings were investigated and the results were compared with those of the conventional decorative chromium coatings. The average grain size of nanocrystalline nickel coatings was determined using X-ray diffraction patterns. Corrosion behaviour was evaluated using electrochemical impedance spectroscopy (EIS) in a 0.6 M sodium chloride solution. A gloss meter and a Suftest device were used to evaluate surface brightness and roughness. Corrosion resistance and brightness of the nanocrystalline nickel coatings increased with increasing the saccharin concentration in the bath. Moreover, brighter nanocrystalline nickel coatings were obtained with increasing the peak current density. In addition, all nanocrystalline nickel coatings were more corrosion resistant than chromium coatings. Those nanocrystalline nickel coatings with average grain sizes of less than 38 nm were brighter and had smoother surfaces than conventional decorative chromium coatings.

Keywords Nanocrystalline nickel · Decorative chromium · Corrosion · Brightness

1 Introduction

Chromium coatings have been used widely for functional purposes in various kinds of industries due to their excellent properties such as high hardness and good resistance to wear and corrosion [1, 2]. They are also used for aesthetic purposes. Bright decorative chromium is plated as a thin layer on a relatively thick layer of nickel to provide a decorative finish, while the function of the underlayer nickel coating is protection against corrosion. However, regarding the environmental concerns, conventional chromium coatings are now considered to be a significant problem. Chromates have been regarded as highly carcinogenic chemicals. The Cr^{+6} ion can react with DNA, forming chromium (V)-glutathione DNA adducts which may be the cause of the tumour-initiating capability of the Cr^{+6} ion and some of its other toxic effects. As a result, electrodeposition of chromium requires specific equipment such as special waste disposal methods and costly breathing apparatus and exhaust systems [3–5]. Thus, it would be reasonable to find an environmental friendly alternative to chromium coatings.

Ni–P coatings obtained by electroless deposition of nickel from solutions containing hypophosphate ions also have desirable properties such as high hardness, good wear resistance and corrosion resistance [6, 7]. However, electroless nickel deposition technique can be an expensive option due to the cost of reducing agents. The nanocrystalline nickel coatings would have different physical and electrochemical properties in comparison with the conventional polycrystalline nickel coatings [8]. One of the most practical techniques by which nanocrystalline coatings can be synthesised is pulse electroplating [9–11]. Grain refining agents such as saccharin have been used in various amounts for further decrease in the grain size of nickel electrodeposits. These additives are absorbed onto the surface and shorten the mean free path for lateral diffusion of ions. Consequently, the coefficient of diffusion is decreased and the concentration of ions at the steady state

P. Najafi Sayar · M. E. Bahrololoom (✉)
Department of Materials Science and Engineering, School of Engineering, Shiraz University, 71348–15939 Shiraz, Iran
e-mail: bahrolom@shirazu.ac.ir

would increase [12]. Previous studies have shown that the corrosion resistance of some materials would be improved as a result of grain size reduction to nano scale [13, 14].

Despite some reports in the literature regarding the corrosion behaviour of nanocrystalline nickel coatings and chromium coatings, there is no evidence of comparing the corrosion behaviour of these two types of coatings with each other. The aim of this study was a comparison between the corrosion behaviour of the nanocrystalline nickel coatings with the conventional chromium coatings, using electrochemical impedance spectroscopy (EIS). Another important property of decorative chromium coatings is its brightness. Thus, brightness and surface roughness of the pulse plated nanocrystalline nickel coating were also compared with those of the decorative chromium coating in order to nominate the former as an environmentally acceptable alternative to the hazardous chromium coatings.

2 Experimental

Nanocrystalline nickel coatings were pulse plated on copper substrates using a Watt's bath which contained 300 g L^{-1} nickel sulphate, 45 g L^{-1} nickel chloride, 45 g L^{-1} boric acid, and saccharin with different concentrations (0, 1, 5, and 10 g L^{-1}). The range of saccharin concentration was selected based on the optimum values that have been reported by previous studies [9–11]. Sulfamate-nickel-antipit (SNAP) was added to the bath, in order to facilitate the removal of hydrogen bubbles from the cathode surface. Nickel was used as the anode. The reason for using different concentrations of saccharin was to produce nanocrystalline nickel deposits with different grain sizes and to evaluate the effect of saccharin concentration on the corrosion behaviour, surface brightness and roughness of these coatings. Nickel pulse-plating was performed with rectangular pulses (t_{on} = 2.5 and 5 ms, t_{off} = 95 and 45 ms) having peak current densities of 2 and 0.3 A cm^{-2} for 10 min at 60 °C and the bath pH of 3–3.5. Chromium was electrodeposited on copper substrates with a lead anode (similar to the anodes used in the industry) and a direct current density of 0.3 A cm^{-2} using a conventional chromic acid bath with a composition of 250 g L^{-1} chromic oxide and 2.5 g L^{-1} sulphuric acid at 55 °C. The bath pH varied over the range of 1 to 1.5 and the deposition time for chromium was 45 minutes. The electroplating processes were controlled in order to have approximately the same thickness for all coatings (Fig. 1a, b).

A Cu Kα radiation at a scan rate of 5°min^{-1} in a Bruker D8 advance diffractometer was used to obtain X-ray diffraction (XRD) patterns of the nanocrystalline nickel coatings. The full width of maximum intensity (FWHM) of the diffraction peaks were estimated by pseudo–voigt curve fitting method. In the case of nanocrystalline materials which have broadening from both lattice microstrain and fine grain size, a combination of Stokes and Wilson formula (the first term in Eq. 1) and Scherrer formula (the second term in Eq. 1) should be used to determine the microstrain and the average grain size [15].

$$W_f = 2\zeta \tan\theta + 0.9\lambda/D\cos\theta \quad (1)$$

where W_f is the FWHM of a Bragg reflection excluding instrumental broadening, λ is the wave length of X-ray radiation, D is the average grain size, θ is the Bragg angle and ζ is the effective lattice microstrain. The microstrain and the average grain size in the nanocrystalline nickel coatings were calculated by linear fitting of X-ray data. The slope and the intercept with $\sin\theta = 0$ of the plot of $W_f \cos\theta$ versus $\sin\theta$ provided the microstrain ζ and the average grain size D, respectively.

Electrochemical impedance tests were performed using a potentiosatat/galvanostat (μAUTOLAB Type III Eco Chemie BV, The Netherlands) equipped with a Frequency

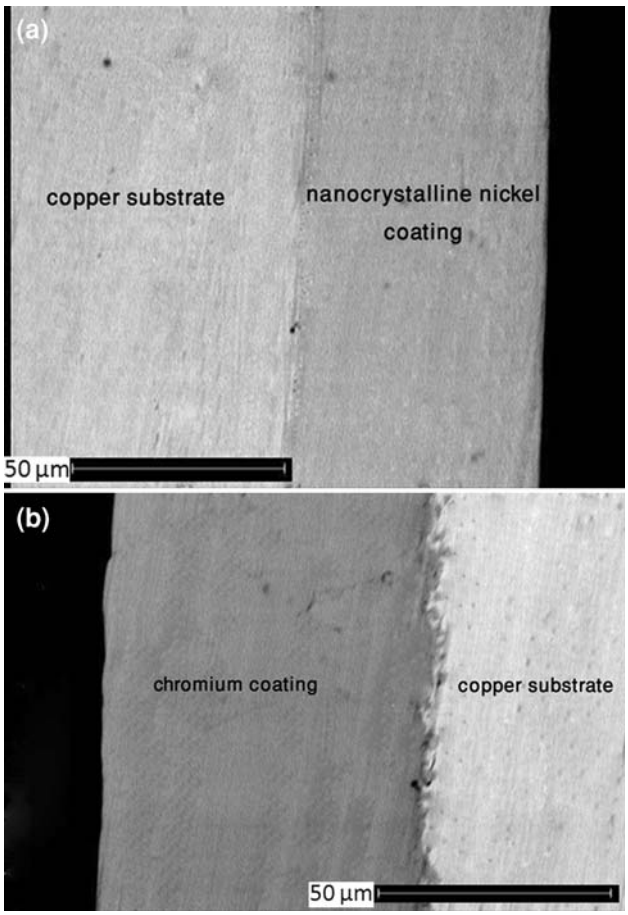

Fig. 1 SEM micrographs of the cross sections of **a** nanocrystalline nickel and **b** chromium coatings

Response Analyser 4.9 and a General Purpose Electrochemical System 4.9 software. A conventional three electrodes Pyrex glass cell was used for these corrosion experiments. Round copper disks, each having an exposed area of 1 cm^2, were coated with chromium and nanocrystalline nickel to be used as the working electrodes. A saturated calomel reference electrode and a platinum counter electrode were used. The aggressive environment was an open to air solution of 0.6 M sodium chloride at 25 °C for all tests. The working electrodes were immersed in a test solution for approximately 45 min prior to each test, in order to establish a stable open circuit potential. Electrochemical impedance spectroscopy (EIS) measurements were made at the corrosion potentials E_c over a frequency range of 100 kHz–10 mHz, with a signal amplitude perturbation of 5 mV.

The surface roughness of each coating was reported as an average value using a Mitutoyo Suftest 201 device. A Xinrui WGG60 mini gloss meter was used to evaluate surface brightness of specimens under 60° reflected light detector angle. The measured values for both surface brightness and roughness tests were taken from two separate measurements on each specimen.

3 Results and discussion

The results of EIS measurements (typical data) for the nanocrystalline nickel coatings and chromium coatings are presented in Figs. 2, 3, and 4 respectively. As seen, decreasing the average grain size of the nanocrystalline nickel coatings resulted in an increase in the size of the Nyquist plots (Fig. 2a–e). Moreover, all Bode plots had resistive regions at high and low frequencies, while capacitive regions occurred at the intermediate frequencies over the tested frequency range (Fig. 3a–e and Fig. 4b). The impedance values were found to be dependent on the average grain size of the nanocrystalline nickel coatings. Decreasing the average grain size resulted in an increase in the impedance of the interface and the maximum phase angle (Fig. 3a–e). These results indicated that the nanocrystalline nickel coatings with smaller grain sizes were more corrosion resistant. In addition, all nanocrystalline nickel coatings exhibited higher impedance of the interface and the maximum phase angle in comparison with the chromium coatings implying that the former had more corrosion resistance than the latter. The impedance data for all coatings in a 0.6 M sodium chloride solution were analyzed using an equivalent circuit model $R_s(Q_{dl}R_p)$. For a homogeneous system with a one-time constant, the transfer function would be represented by a solution resistance (R_s) coupled with a capacitor (C) which is parallel with charge transfer resistance (R_P) [16].

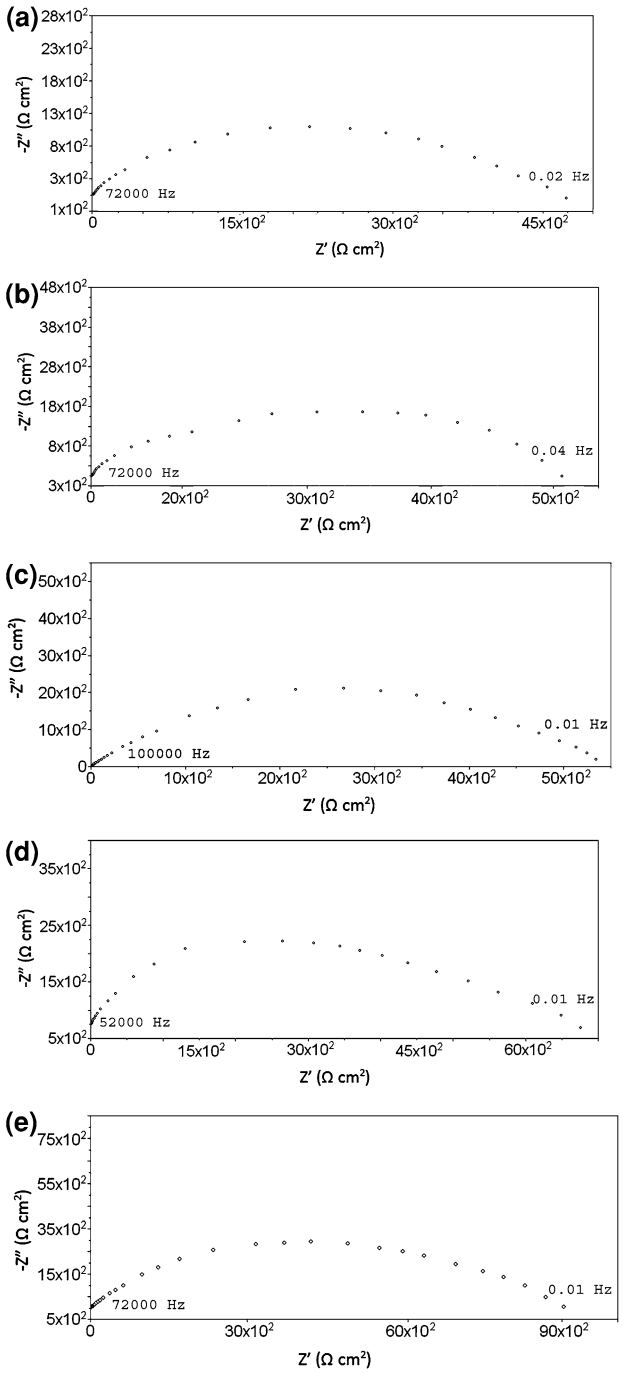

Fig. 2 **a–e** The Nyquist plots of nanocrystalline nickel coatings with grain size of 438, 38, 32, 22, 15 nm, respectively, in a 0.6 M sodium chloride solution

$$Z_{(w)} = R_S + (1/R_P + iCw)^{-1}. \quad (2)$$

However, when the frequency response is non-ideal, then Eq. 2 cannot serve as a transfer function and the capacitor is replaced by a constant phase element (CPE). The impedance (Z) of the CPE is then:

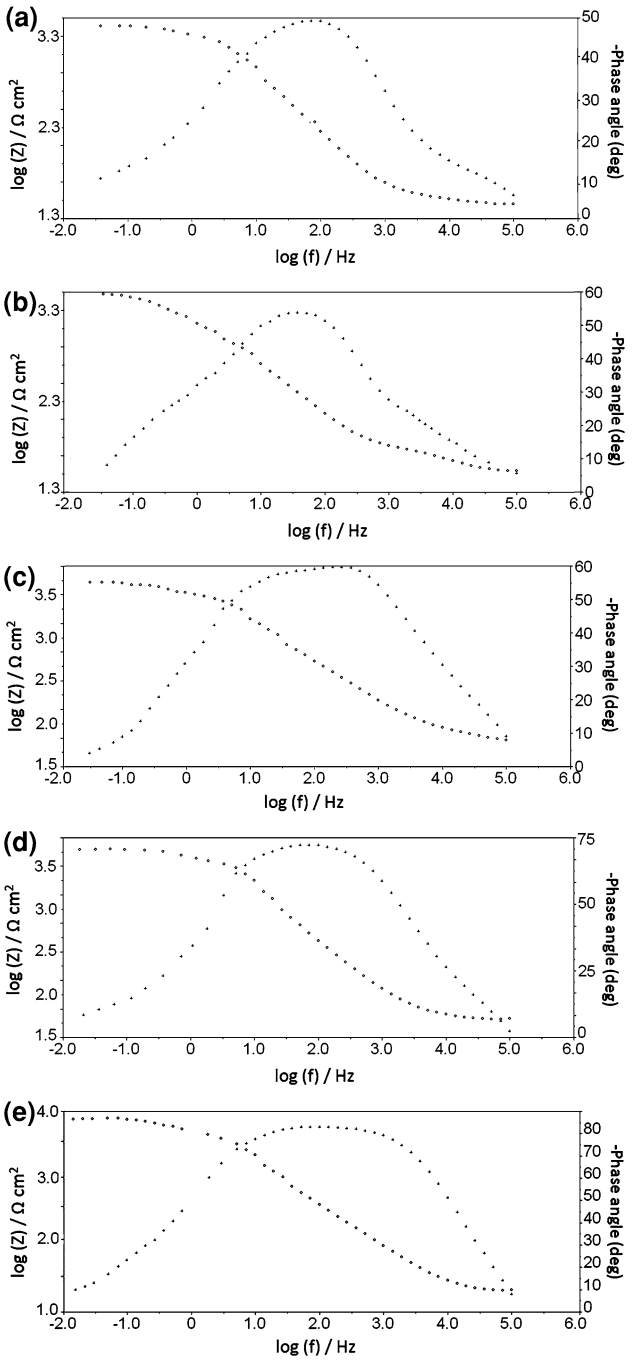

Fig. 3 **a–e** The Bode plots of nanocrystalline nickel coatings with grain size of 438, 38, 32, 22, 15 nm, respectively, in a 0.6 M sodium chloride solution

$$Z = 1/Q(iw)^n \tag{3}$$

in which, $i = (-1)^{1/2}$ is an imaginary number, $w = 2\pi f$ is the angular frequency in rad s^{-1}, where f is the frequency in Hertz, Q is a constant and n is an empirical exponent, which varies between 0 for a perfect resistor and 1 for a perfect capacitor. The corresponding electrochemical parameters are presented in Table 1. The true capacitance

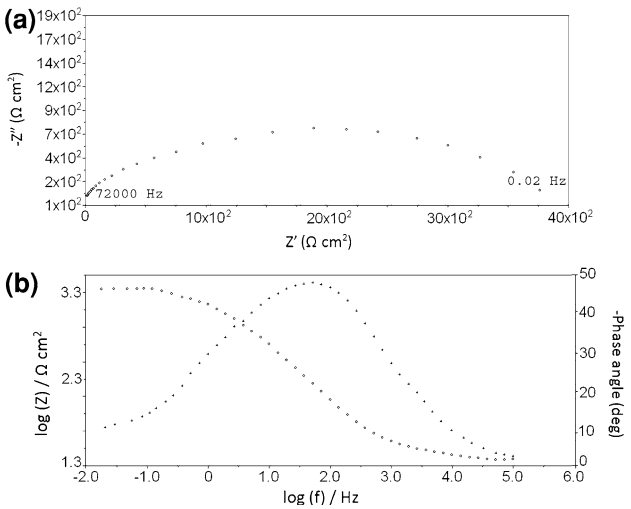

Fig. 4 **a** Nyquist, **b** Bode plots of decorative chromium coatings in a 0.6 M sodium chloride solution

values (Table 1) were calculated from the following equation

$$C = Q(w_{\max})^{n-1} \tag{4}$$

in which $w_{\max}$ is the frequency of the maximum imaginary impedance. The true capacitance is equal to CPE, if $n = 1$ and the CPE capacitance characteristics diminish when n approaches zero [17]. The parameter n is generally accepted to be a measure of surface inhomogeneity [18]. Capacitance values can be used to explain the type of process associated with each time constant. Generally, corrosion time constants have capacitance values in the range of 1 to 20 μF cm^{-2} while capacitance values of more than 100 μF cm^{-2} are believed to occur when diffusion or surface adsorption occurs in conjunction with corrosion [17]. Thus, according to the capacitance values (Table 1), the low frequency time constants in Figs. 2 and 4 are due to the corrosion phenomenon only. In addition, the accuracy of the selected equivalent circuit model was estimated using residuals plot. A model is a good fit to the experimental data when the number of positive residual values is approximately equal to the number of negative values. The validity of the model should be questioned when significantly more residual values are above or below zero or periodicity of residuals is observed around zero. [19] As seen from the residuals plots (Fig. 5a–f), the equivalent circuit model was selected with a reasonable fit to the experimental data. It can be seen from Table 1 that charge transfer resistance (R_P) for the nanocrystalline nickel coatings increases as the saccharin concentration in the nickel bath increases. This indicates that the corrosion susceptibility of the nanocrystalline nickel coatings decreases with increasing the saccharin concentration in the bath. The effect of microstrain present in the

Table 1 Impedance parameters for nano-Ni and chromium coatings in 0.6 M sodium chloride solution

Type of coating	PDS (A cm^{-2})	SC (g L^{-1})	D (nm)	E_c (V)	R_S (Ω cm^2)	R_P (KΩ cm^2)	Q (Ω^{-1} s^n cm^{-2} $\times$ 10^{-5})	C (F cm^{-2} $\times$ 10^{-5})	n
Nano-Ni	0.3	0	438	−0.51 ± 0.02	32.5 ± 1.05	4.54 ± 0.11	1.42 ± 0.09	1.32 ± 0.08	0.85 ± 0.01
Nano-Ni	0.3	10	38	−0.49 ± 0.03	34.1 ± 2.51	5.13 ± 0.36	1.33 ± 0.14	1.22 ± 0.13	0.92 ± .0.20
Nano-Ni	2	1	32	−0.32 ± 0.01	35.4 ± 1.36	5.36 ± 0.19	1.21 ± 0.07	1.11 ± 0.06	0.92 ± 0.01
Nano-Ni	2	5	22	−0.31 ± 0.02	30.2 ± 1.21	6.08 ± 0.46	1.19 ± 0.10	1.08 ± 0.09	0.92 ± 0.01
Nano-Ni	2	10	15	−0.26 ± 0.01	28.7 ± 1.28	9.23 ± 0.28	1.13 ± 0.07	1.07 ± 0.06	0.94 ± 0.01
Chromium	0.3	–	–	−0.54 ± 0.01	28.9 ± 0.62	3.59 ± 0.13	1.65 ± 0.07	1.85 ± 0.08	0.88 ± 0.01

PDS peak current density, *SC* saccharin concentration, *D* average grain size, E_c corrosion potential at which EIS measurements were made

nanocrystalline nickel coatings on their corrosion behaviour has been reported [20]. The results of microstarin calculations from the XRD data for nanocrystalline nickel coatings (Fig. 6) are listed in Table 2. The equation of the $W_f \cos\theta$ as a function of $\sin\theta$ is presented in this table. The nature of plots indicates that all nanocrystalline nickel coatings bear compressive strain. Increasing the saccharin concentration in the nickel bath enhances the lattice microstrain in nanocrystalline nickel coatings which can be attributed to the higher sulphur content with saccharin addition [20]. Also, it has been shown that compressive strains in nanocrystalline nickel coatings retard their anodic dissolution [20]. So, adding more saccharin to the nickel bath leads to more corrosion resistant nickel coatings.

A comparison between the charge transfer resistance of nanocrystalline nickel coatings and that of the chromium coating (Table 1) indicates that the corrosion resistance of the nanocrystalline nickel coating is superior to that of the conventional chromium. It seems that separate zones with anodic (dissolution) and cathodic reactions are formed initially on a nickel or chromium coating which is immersed into NaCl solutions. Study of the surface morphology of these coatings after corrosion showed that corrosion was not uniform. As shown in Fig. 7a, different zones (dark and bright patches) were formed on the chromium coating after corrosion. The dark patches could be the corrosion products formed on the anodic zones and the bright areas seem to be the cathodic zones on the chromium coatings which were not corroded. Similar phenomenon was also observed for the nickel coatings after corrosion. As seen in Fig. 7b, the dark grey and black areas could be those parts of the nickel coating which were corroded (the anodic zones). In contrast, the cathodic zones which were not dissolved due to corrosion are seen as white and light grey globular structures, indicating that corrosion was not uniform. Q values are associated with the surface area available for the cathodic reaction [21]. The Q values of nanocrystalline nickel coatings decreased with increasing the saccharin concentration. According to the data, calculated from the XRD patterns of nanocrystalline nickel coatings (Table 2), increasing the saccharin concentration in the bath resulted in decreasing the average grain size in the nanocrystalline nickel coatings. Similar behaviour has been reported by other researchers [9, 22]. Thus, with more saccharin in the bath, the surface density of grain boundaries in the coating increases. Atoms in grain boundaries have lower residual cohesive energy and consequently they possess more energy and exist in an unstable state [23]. As a result, increasing the saccharin concentration in the bath would cause a decrease in the surface area available for cathodic reactions and hence diminish the Q values. As seen from n values of nanocrystalline nickel coatings (Table 1), increasing the saccharin concentration in the electroplating bath results in n values closer to unity, in other words, the surface roughness of nanocrystalline nickel coatings decreases with increasing the saccharin concentration in the bath. In addition, a comparison between the n values of nanocrystalline nickel coatings and that of chromium indicates that the surface roughness of the chromium coating was higher than that of nanocrystalline nickel coatings which have grain size less than 38 nm. These results are in good agreement with the surface roughness data presented in Fig. 9.

Long term corrosion stability of these coatings was estimated as follows. The Stern and Grey relationship (Eq. 5) was used to convert the corrosion resistance to the corrosion current as follows:

$$i_{corr} = \left(1/2.303R_p\right) \times (\beta_a \times \beta_c)/(\beta_a + \beta_c). \quad (5)$$

In which, i_{corr} is the corrosion current density in μA cm^{-2}, (R_P) is the corrosion resistance in Ω cm^2, β_a is the anodic Tafel slope and β_c is the cathodic Tafel slope in V/decade. To estimate the service lifetime of a metal structure, corrosion currents can be converted to the corrosion rates by the following equation

$$\text{MPY} = i_{corr}(\Lambda\varepsilon/\rho) \quad (6)$$

where Λ is a combination of several conversion terms, which is equal to 1.2866×10^5 (equivalents.sec.mils)/(Colombs.cm.year), i_{corr} is the corrosion current density in

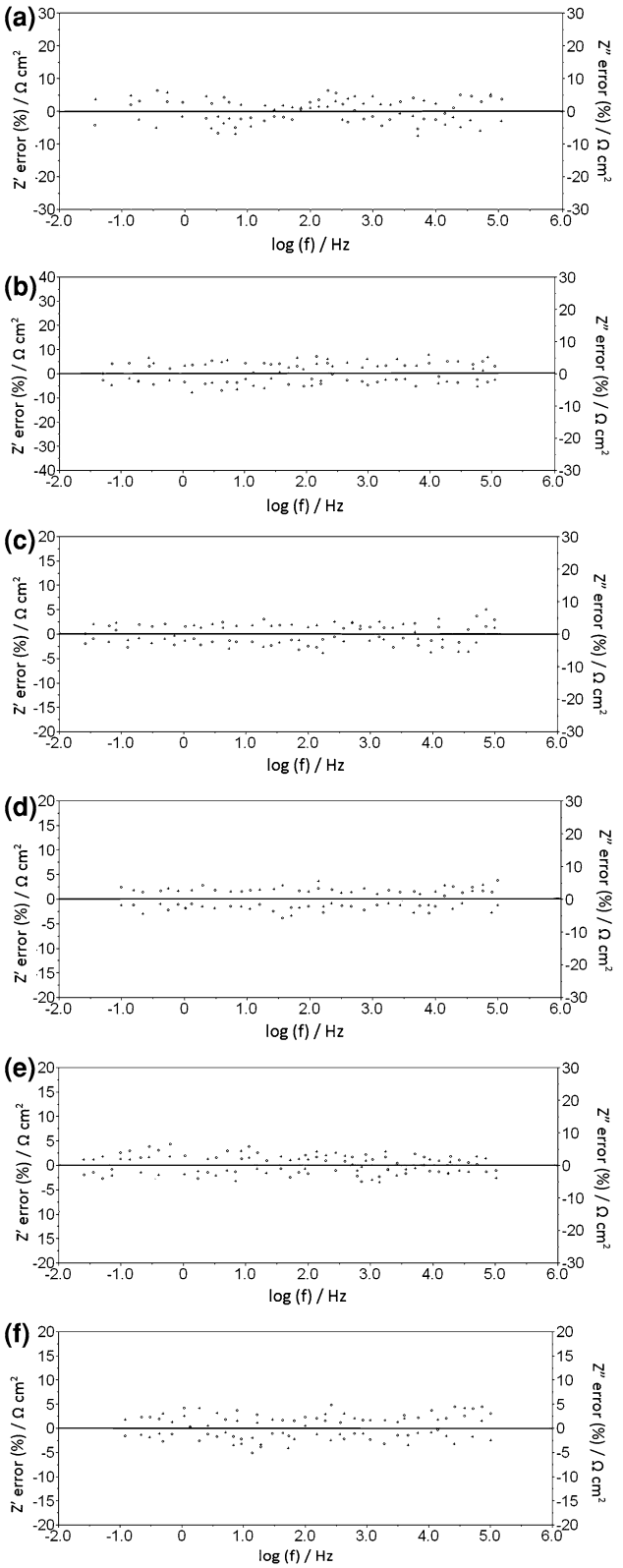

Fig. 5 The impedance residuals plot for **a, b, c, d, e** nanocrystalline nickel coatings with grain size of 438, 38, 32, 22, 15 nm, respectively, and **f** chromium coatings in a 0.6 M NaCl solution

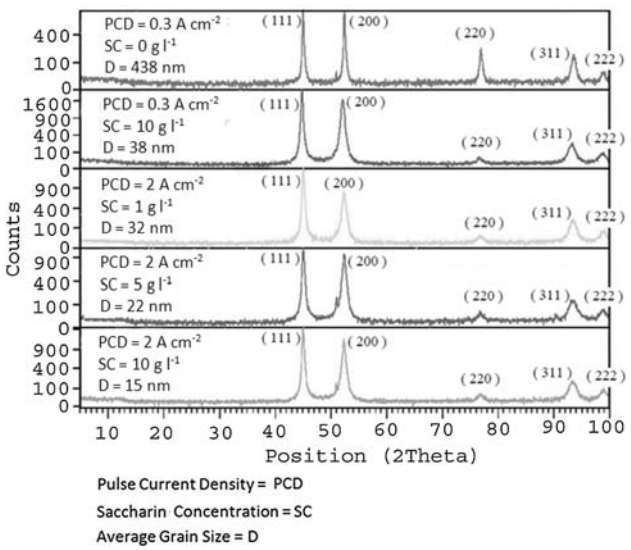

Fig. 6 The X-ray diffraction patterns of nanocrystalline nickel coatings pulse plated at various operational conditions

A cm^{-2}, ρ is the metal density and ε is the equivalent weight in g/equivalent. [24] The results of these calculations are summarised in Table 3.

Surface brightness values for the nanocrystalline nickel which were pulse plated at various operational conditions are illustrated in Fig. 8 and compared with that of the conventional decorative chromium. As the saccharin concentration in the bath increases the surface brightness of the nanocrystalline nickel coatings increases. According to the X-ray diffraction patterns of nanocrystalline Nickel coatings (Fig. 6), the preferred orientation of the deposits changed from (111), (200) and (220) fibre texture for a saccharin free bath to a (111) and (200) double fibre texture for the saccharin containing baths. This result is in agreement with the observations reported by previous studies [20, 23]. Some researchers related this phenomenon to the decrease in the grain size, crystallographic anisotropy, surface energy, and nucleation rate [25, 26]. It is obvious from Fig. 8 that if sufficient amount of saccharin is added to the bath (i.e. 10 g L^{-1}) brighter nanocrystalline nickel coatings (with respect to the conventional decorative chromium) can be produced using high (2 A cm^{-2}) or low (0.3 A cm^{-2}) peak current densities. Also, nanocrystalline nickel coatings with the average grain size less than 38 nm have brighter surfaces than the conventional decorative chromium. According to a recent report by Bayramoglu et al., the brightness of chromium plating increases with increasing chromic acid concentration in the bath. This might be due to the fact that fine crystal sizes are required to electrodeposit the brightest chromium coatings, and these are achieved from the baths with high chromic acid

Table 2 Estimated grain size and microhardness of the nanocrystalline nickel deposits

PCD (A cm^{-2})	SC (g L^{-1})	$W_f \cos\theta = 2\zeta \sin\theta + 0.9\lambda/D$	D (nm)	Microstarin $\times 10^{-3}$
0.3	0	$Y = -4.3 \times 10^{-5}X + 3.2 \times 10^{-4}$	438	0.0022
0.3	10	$Y = -2.1 \times 10^{-3}X + 3.7 \times 10^{-3}$	38	1.05
2	1	$Y = -3.2 \times 10^{-3}X + 4.3 \times 10^{-3}$	32	1.6
2	5	$Y = -4.7 \times 10^{-3}X + 6.3 \times 10^{-3}$	22	2.4
2	10	$Y = -8.6 \times 10^{-3}X + 9.5 \times 10^{-3}$	15	4.3

PDS peak current density, *SC* saccharin concentration, *D* average grain size

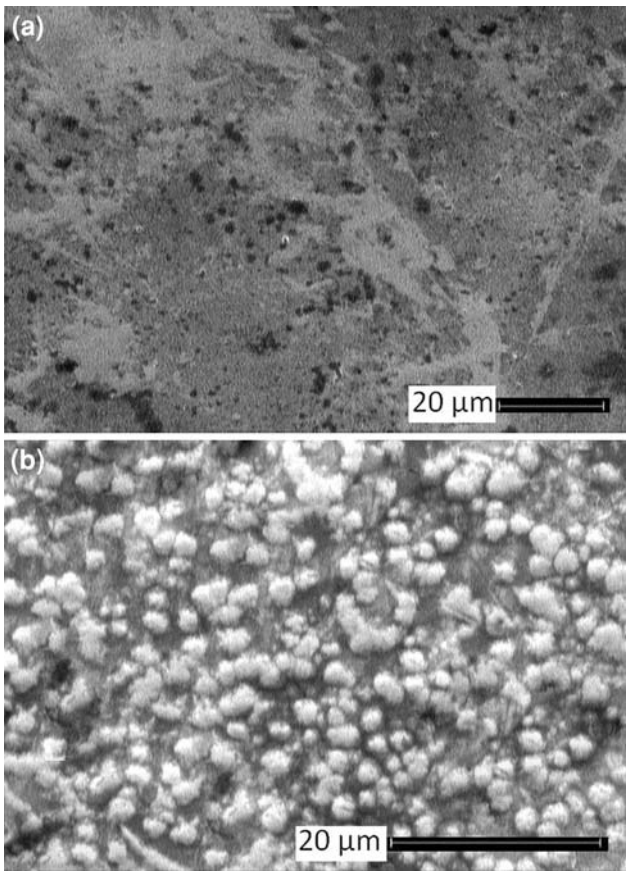

Fig. 7 SEM micrographs of **a** chromium and **b** nanocrystalline nickel coatings after corrosion tests

concentrations [27]. In other words, to electrodeposit brighter chromium coatings, more hazardous baths have to be used. Thus, nanocrystalline nickel coatings which were studied here can be a good alternative to bright decorative chromium coatings. Furthermore, a decorative chromium coating is usually electroplated on a nickel underlayer protective coating while the function of the chromium top layer is mainly aesthetic due to its brightness. Consequently, nanocrystalline nickel coatings with equal brightness as decorative chromium coatings can eliminate the process of chromium plating which is hazardous to the environment.

The average surface roughness of nanocrystalline nickel coatings are compared with that of the conventional decorative Chromium in Fig. 9. As seen, the surface roughness of nanocrystalline nickel coatings decreases as the saccharin concentration in the bath increases. This result is in agreement with the surface brightness values presented in Fig. 8, indicating that specimens with less surface roughness are brighter than the coatings with higher roughness values. Generally, brightness can be attributed to low surface roughness and small grain size. The present investigation showed that these physical characteristics were present in the pulse plated nanocrystalline nickel coatings.

4 Conclusions

As the grain size of nanocrystalline nickel coatings diminishes (from 438 to 15 nm), the corrosion resistance enhances, the surface heterogeneity decreases and the surface area available for cathodic reactions decreases too. In addition, all nanocrystalline nickel coatings with various grain sizes (in the range of 438 to 38 nm) exhibit more corrosion resistance than the chromium coating. As the saccharin concentration in the nickel bath increases (from 0

Table 3 Long term corrosion stability of nanocrystalline nickel and decorative chromium coatings in 0.6 M NaCl solution

Type of coating	PDS (A cm^{-2})	SC (g L^{-1})	D (nm)	R_P (KΩ cm^2)	β_a (V/decade)	β_c (V/decade)	i_{corr} (μA cm^{-2})	MPY
Nano-Ni	0.3	0	438	4.54 ± 0.11	0.09 ± 0.002	0.18 ± 0.004	5.72 ± 0.008	2.43 ± 0.004
Nano-Ni	0.3	10	38	5.13 ± 0.36	0.10 ± 0.005	0.18 ± 0.009	5.44 ± 0.01	2.31 ± 0.05
Nano-Ni	2	1	32	5.36 ± 0.19	0.09 ± 0.004	0.15 ± 0.004	4.55 ± 0.02	1.93 ± 0.008
Nano-Ni	2	5	22	6.08 ± 0.46	0.11 ± 0.003	0.13 ± 0.006	4.25 ± 0.15	1.80 ± 0.06
Nano-Ni	2	10	15	9.23 ± 0.28	0.09 ± 0.002	0.11 ± 0.003	2.32 ± 0.005	0.98 ± 0.003
Chromium	0.3	–	–	3.59 ± 0.13	0.11 ± 0.002	0.17 ± 0.004	8.07 ± 0.12	2.51 ± 0.04

PDS peak current density, *SC* saccharin concentration, *D* average grain size

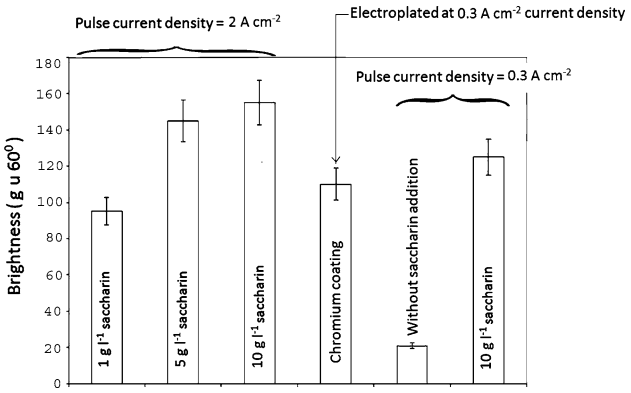

Fig. 8 Comparison of the surface brightness in chromium coatings with those of nanocrystalline nickel coatings

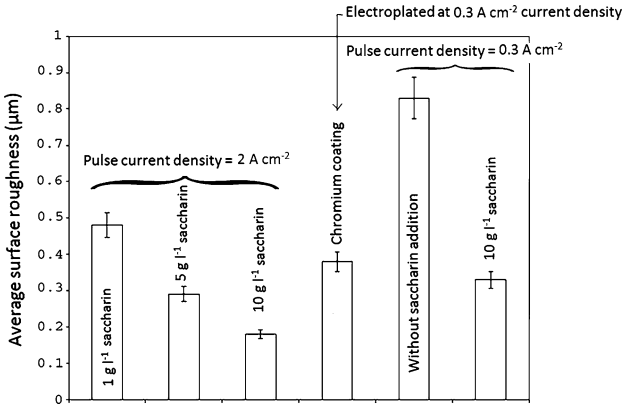

Fig. 9 Comparison of the surface roughness in chromium coatings with those of nanocrystalline nickel coatings

to 10 g L^{-1}) the surface roughness of nanocrystalline nickel coatings decreases and their surface brightness increases. Moreover, nanocrystalline nickel coatings with an average grain size of less than 38 nm can be brighter than conventional chromium coatings.

Acknowledgement The financial support for this research (grant number 86-GR-ENG-62) given to Dr. M.E. Bahrololoom by the Research Committee of Shiraz University is gratefully appreciated.

References

1. Zeng Z, Wang L, Liang A, Zhang J (2006) Electrochim Acta 52:1366
2. Wang L, Gao Y, Xue Q, Liu H, Xu T (2006) Surf Coat Technol 200:3719
3. Baral A, Engelken R, Stephens W, Farris J, Hannigan R (2006) Arch Environ Contam Toxicol 50:496
4. Lindberg E, Hedensteirna G (1983) Arch Environ Health 38:367
5. Eskin S, Berkh O, Rogalsky G, Zahavi J (1998) Plat Surf Finish 85:79
6. Hady H, Abdel Salam OF (2008) J Appl Electrochem 38:385
7. Khan E, Oduoza CF, Pearson T (2007) J Appl Electrochem 37:1375
8. Ebrahimi F, Bourne GR, Kelly MS, Matthews TE (1999) Nanostruct Mater 11:343
9. Erb U (1995) Nanostruct Mater 6:533
10. Moti E, Shariat MH, Bahrololoom ME (2008) Mater Chem Phys 111:469
11. Moti E, Shariat MH, Bahrololoom ME (2008) J Appl Electrochem 38:605
12. Mishra R, Basu B, Balasubramaniam R (2004) Mater Sci Eng A 373:370
13. Cherkaoui M, Chassaing E, Vu Quang K (1988) Surf Coat Technol 34:243
14. Zimmerman AF, Clark DG, Aust AT, Erb U (2002) Mater Lett 52:85
15. Klug HP, Alexander LE (1974) X-ray diffraction procedures for polycrystalline and amorphous materials. Wiley, New York
16. Popova A, Christov M (2006) Corr Sci 48:3208
17. Bard AJ, Falkner LR (1980) Electrochemical methods, fundamentals and applications. Wiley, New York
18. Drogowska M, Bossard L, Menard H, Lasia A (1995) Mater Sci Forum 192:89
19. Darper N, Smith H Jr (1981) Applied regression analysis, 2nd edn. Wiley, New York
20. Mishra R, Balasubramaniam R (2004) Corr Sci 46:3019
21. Lopez DA, Simison SN, de Sanchez SR (2003) Electrochim Acta 48:845
22. El-Sherik AM, Erb U (1995) J Mater Sci 38:5743
23. Yong P, Yi-chun Z, Zhao-feng Z, Yong-li H, Yan-guo L, Chang-qing S (2007) Trans Nonferr Metal Soc China 17:1225
24. Mansfeld F (1986) Electrochemical methods. NACE, Houston, TX
25. Nakamura Y, Kaneko N, Watanabe M, Hezu H (1994) J Appl Electrochem 24:227
26. Li H, Czerwinski F, Szpunar A (1997) Nanostruct Mater 9:673
27. Bayramoglu M, Onet B, Geren N (2008) J Mater Process Tech 203:277